International Journal of Thermal Sciences 48 (2009) 1510–1516

Contents lists available at ScienceDirect

International Journal of Thermal Sciences

www.elsevier.com/locate/ijts

Determination of thermal radiative properties of packed-bed media containing a mixture of polydispersed particles

Klaus Jäger [a], Wojciech Lipiński [b], Helmut G. Katzgraber [a,c], Aldo Steinfeld [d,e,*]

[a] Theoretische Physik, ETH Zurich, CH-8093 Zurich, Switzerland
[b] Department of Mechanical Engineering, University of Minnesota, Minneapolis, MN 55455, USA
[c] Department of Physics, Texas A&M University, College Station, TX 77843-4242, USA
[d] Department of Mechanical and Process Engineering, ETH Zurich, 8092 Zurich, Switzerland
[e] Solar Technology Laboratory, Paul Scherrer Institute, 5232 Villigen, Switzerland

ARTICLE INFO

Article history:
Received 8 July 2008
Received in revised form 6 November 2008
Accepted 16 December 2008
Available online 14 January 2009

Keywords:
Radiation
Packed bed
Radiative properties
Monte Carlo
Spectroscopy
Solar energy

ABSTRACT

Thermal radiative characteristics of packed beds containing a mixture of polydispersed SiO_2, ZnO, and C particles are determined numerically by employing the Monte Carlo technique, which is validated with the experimentally measured overall transmittance. A radiative heat transfer model is formulated for a pseudo-continuum multi-component medium of Mie-scattering particles. Good agreement is achieved by incorporating approximate phase functions that reproduce the experimentally observed preference for forward scattering.

1. Introduction

Packed beds containing reacting particles exposed to high-flux irradiation are encountered in thermochemical applications that make use of concentrated solar energy as the source of high-temperature process heat [1–5]. These packed beds, which often involve particles of metal oxides, carbonaceous materials, and other highly-attenuating materials, are characterized by their low effective thermal conductivity, which leads to large temperature gradients and, consequently, to a non-uniform rate of chemical reaction. Thus, heat transfer within the packed bed becomes the limiting controlling mechanism and affects the energy conversion efficiency of the solar thermochemical process. Of special interest is the carbothermic reduction of ZnO at above 1200 K, performed in a shrinking packed bed exposed to intense thermal radiation incident from the top under conditions that are typical of ablation processes [3]. Experimental radiation measurements and associated numerical Monte Carlo simulations of a packed-bed ZnO/C mixture revealed a short mean free path of radiation propagation through this material [6]. In a following study, it was shown experimentally that adding large (>100 μm) semi-transparent SiO_2 particles can significantly reduce the optical thickness, and consequently, enhance the radiative heat transfer within the packed-bed [7]. Previous pertinent studies of the radiative properties in particulate media include a review of experimental work up to 1991 and scattering analysis of collimated radiation [8], experimental characterization of radiative properties of disperse systems [9], experimental determination of the extinction coefficient of packed-beds [10–13] and dense media [14,15], and Monte Carlo-based determination of radiative characteristics of packed beds of large particles [16–18].

In the present paper, thermal radiative properties of packed-beds containing polydispersed SiO_2, ZnO and C particles are determined by applying the Monte Carlo technique, which is validated by comparing numerically computed and experimentally measured overall transmittance.

2. Experimental set-up

The experimental set-up and methodology have been previously described in detail [7]; only the principal features are summarized here and shown schematically in Fig. 1. The main hardware components are: (#1) a 5 mW He–Ne laser as a source of monochromatic radiation at 632.8 nm; (#2) a fiber optic of 400 μm diameter; (#3) a convex BK7 lens of 20 mm-width and 50 mm-focal length; (#4) a 6 mm diameter diaphragm; (#5) a sample placed inside a holder consisting of 20 mm-internal diameter steel rings mounted on top of a 3.3 mm-thick 50 mm-di-

* Corresponding author at: Department of Mechanical and Process Engineering, ETH Zurich, 8092 Zurich, Switzerland. Tel.: +41 44 6327929.
E-mail address: aldo.steinfeld@eth.ch (A. Steinfeld).

1290-0729/$ – see front matter
doi:10.1016/j.ijthermalsci.2008.12.006

Nomenclature

A, B	parameters in Eqs. (1) and (2)
a	particle radius ..... m
f	volumetric particle size distribution function ... m^{-1}
f_v	particle volume fraction
i	medium component index, $i = SiO_2$, ZnO, and C
j	index in Eq. (2)
k	index of a scattering component in Eqs. (11) and (12)
m	complex refractive index, $m = n - ik$
n	number of medium components
n_p	particle size distribution function ..... m^{-1}
N	number of stochastic rays in MC
Q	efficiency factor
$\dot{Q}$	heat transfer rate, power ..... W
s	path length ..... m
T	overall transmittance
x_i	mass fraction of component i

Greek symbols

β	extinction coefficient ..... m^{-1}
γ	parameter in Eqs. (1) and (2)
Δ	thickness of a packed-bed sample ..... m
ζ	forward-scattering amplification factor for ZnO
δ	parameter in Eqs. (1) and (2)
θ	cone (polar) angle ..... rad
κ	absorption coefficient ..... m^{-1}
λ	wavelength ..... m
ξ	particle size parameter
ρ	density ..... $kg\,m^{-3}$
σ	Stefan-Boltzmann constant, $\sigma = 5.6704 \cdot 10^{-8}\ W\,m^{-2}\,K^{-4}$
σ_{sca}	scattering coefficient ..... m^{-1}
Φ	scattering phase function
φ	circumferential (azimuthal) angle ..... rad
ω	scattering albedo

Other symbols

$\Re$	random number from a uniform distribution (0, 1)

Subscripts

abs	absorption
b	bulk
C	carbon
exp	experimental
ext	extinction
in	incident
p	particle
r	radiative
refr	refracted
sca	scattering
SiO_2	silicon dioxide (quartz)
ZnO	zinc oxide
λ	spectral

Superscripts

m	mixture

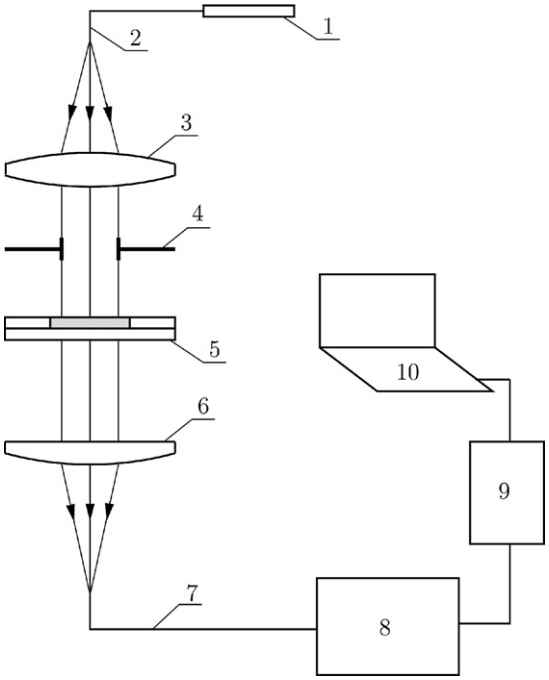

Fig. 1. Experimental set-up: 1–He–Ne laser light, 2–fiber optic, 3–collimating lens, 4–diaphragm, 5–sample holder, 6–collecting lens, 7–fiber optic, 8–spectrometer equipped with an Si detector and an optical chopper, 9–lock-in amplifier, 10–PC data acquisition.

ameter CDAR™-coated glass window; (#6) a MgF_2-coated BK7 lens of 18 mm-width and 72 mm-focal length; (#7) a fiber optic of 800 μm diameter (400 μm core) and 11° cone acceptance angle; (#8) a Triax 320 spectrometer equipped with a Si detector and an optical chopper; (#9) a lock-in amplifier; and (#10) a PC data acquisition system.

Table 1
Particle density, bulk density, volume fraction, and parameters of volumetric size distribution functions of unmixed SiO_2, ZnO and C powders.

i		$\rho_{p,i}$ ($kg\,m^{-3}$)	$\rho_{b,i}$ ($kg\,m^{-3}$)	$f_{v,i}$	A	B	γ	δ
SiO_2		2250	1300	0.577	$1.0474 \cdot 10^{18}$	$1.6069 \cdot 10^{4}$	0.784	1
ZnO		5559	731.4	0.132	$8.6959 \cdot 10^{38}$	$8.8772 \cdot 10^{2}$	1.6189	0.2887
C	$j = 1$	1507	323.6	0.215	$1.0653 \cdot 10^{21}$	$4.2176 \cdot 10^{5}$	0.2351	1
	$j = 2$				$5.6173 \cdot 10^{44}$	$4.4486 \cdot 10^{2}$	4.0963	0.2841

Three powder materials were used to prepare the samples: SiO_2 (crushed natural silica), ZnO (Grillo Nr. 2011), and C (Chemviron, beech charcoal powder). Table 1 lists particle and bulk densities, and volume fractions. Fig. 2 shows volumetric particle size distribution functions $f_i(a)$ normalized according to $\int_0^\infty f_i(a)\,da = 1$,

– for $i = SiO_2$ and ZnO,

$$f_i(a) = \frac{4\pi}{3 f_{v,i}} A_i a^{\gamma_i+3} \exp\left(-B_i a^{\delta_i}\right), \tag{1}$$

– for i = C,

$$f_i(a) = \frac{4\pi}{3 f_{v,i}} \sum_{j=1}^{2} A_j a^{\gamma_i+3} \exp\left(-B_j a^{\delta_i}\right), \tag{2}$$

where $f_{v,i}$ is the volume fraction of the unmixed component i, shown in Table 1. Parameters A, B, γ, and δ were obtained by using the non-linear least-square Levenberg–Marquardt algorithm to fit Eqs. (1) and (2) to the experimentally measured values [19]. They are listed in Table 1. Measurements were performed by laser granulometry for ZnO (Cilas 715, ARP GmbH), by laser scattering

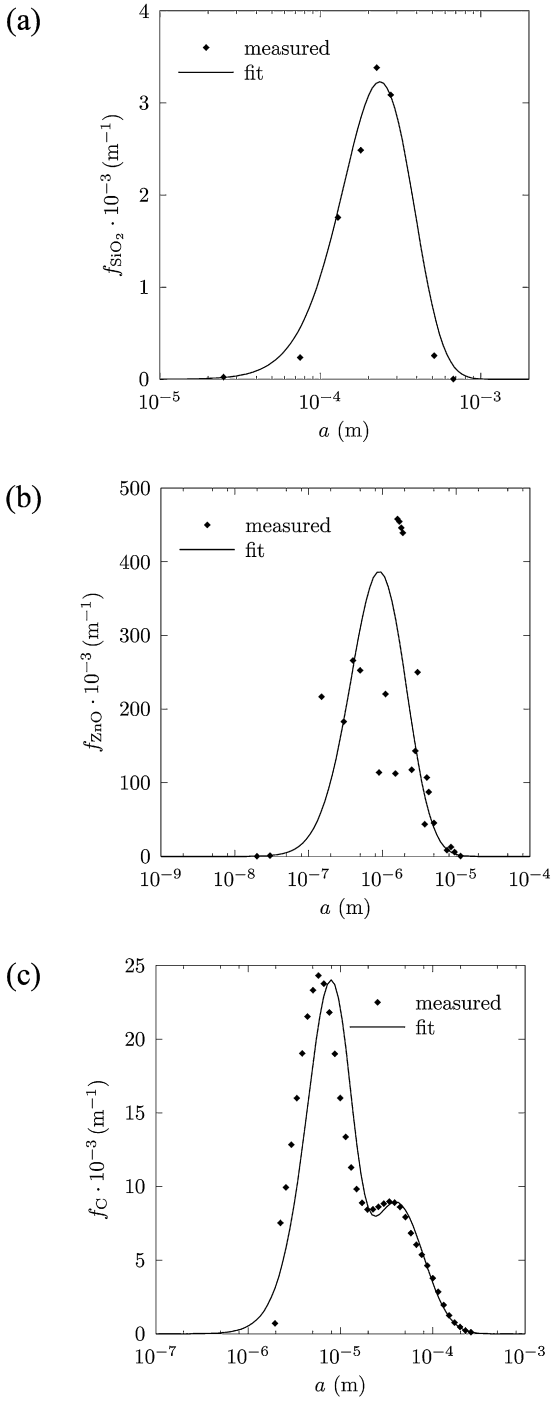

Fig. 2. Particle size distributions of SiO_2, ZnO, and C powders.

particle size analysis for C (Horiba LA-950) and by sieving for SiO_2. The Sauter mean particle radii, calculated by using the fitted functions $f_i(a)$ as,

$$a_{32,i} = \frac{\int_0^\infty f_i(a)\,\mathrm{d}a}{\int_0^\infty a^{-1} f_i(a)\,\mathrm{d}a} = \frac{\int_0^\infty a^3 n_{\mathrm{p},i}(a)\,\mathrm{d}a}{\int_0^\infty a^2 n_{\mathrm{p},i}(a)\,\mathrm{d}a}, \tag{3}$$

are 235.5, 0.9 and 39.6 μm for SiO_2, ZnO and C, respectively, which, at $\lambda = 632.8$ nm, correspond to particle size parameters $\xi \equiv 2\pi a/\lambda$ of 2338, 9.04 and 393, respectively. The medians a_{50} of the measured three distributions are 227.4, 1.8 and 44.7 μm, respectively, corresponding to $\xi = 2258$, 17.87 and 444, respectively. The compositions of the packed-bed mixture samples are listed in Table 2.

Table 2
Composition of the samples.

Sample	Composition (mass %)	x_{SiO_2}	x_{ZnO}	x_C	ρ_b^m (kg m^{-3})
1	100% SiO_2	1	0	0	1300
2	5% ZnO in SiO_2	0.95	0.05	0	1251
3	10% ZnO in SiO_2	0.9	0.1	0	1206
4	2.5% ZnO + C in SiO_2	0.975	0.02206	0.00294	1267
5	7.5% ZnO + C in SiO_2	0.925	0.06618	0.00882	1206

Note that the molar ratios ZnO:C for samples #4 and #5 are the same and equal to 1:0.9.

3. Radiative properties of polydispersed SiO_2, ZnO, and C particles

In the first approach, radiative properties of SiO_2, ZnO, and C powders were computed by applying the Mie theory to polydispersed particles of component i in the packed-bed mixture, and assuming independent scattering by referring to the independent-dependent scattering regime map by Tien and Drolen for the range of particle volume fractions and mean size parameters pertinent to this study [20,22–24]. Thus, the absorption, scattering and extinction coefficients, and the scattering phase function are calculated as[1]

$$\begin{aligned}\{\kappa_i^m, \sigma_{\mathrm{sca},i}^m, \beta_i^m\} &= 0.75 f_{v,i}^m \int_0^\infty \frac{\{Q_{\mathrm{abs},i}(a), Q_{\mathrm{sca},i}(a), Q_{\mathrm{ext},i}(a)\}}{a} f_i(a)\,\mathrm{d}a \\ &= 0.75 f_{v,i}^m \frac{\int_0^\infty \{Q_{\mathrm{abs},i}(a), Q_{\mathrm{sca},i}(a), Q_{\mathrm{ext},i}(a)\} a^2 n_{\mathrm{p},i}(a)\,\mathrm{d}a}{\int_0^\infty a^3 n_{\mathrm{p},i}(a)\,\mathrm{d}a},\end{aligned} \tag{4}$$

$$\Phi_i(\theta) = \frac{0.75 f_{v,i}^m}{\sigma_{\mathrm{sca},i}^m} \int_0^\infty \frac{Q_{\mathrm{sca},i}(a)\Phi_i(a,\theta)}{a} f_i(a)\,\mathrm{d}a, \tag{5}$$

where $f_{v,i}^m$ is the actual volume fraction of component i in the mixture, calculated as

$$f_{v,i}^m = \frac{x_i \rho_b^m}{\rho_{\mathrm{p},i}}, \tag{6}$$

x_i is the mass fraction of component i, $\sum_i x_i = 1$, shown in Table 2, and ρ_b^m is the bulk density of a sample. Refractive indices used were $m_{SiO_2} = 1.457$, $m_{ZnO} = 1.988–5.33 \cdot 10^{-5}$i, $m_C = 1.775–0.508$i [25–27]. The integrals in Eqs. (5) and (6) are computed using Romberg's method [28]. Q_{abs}, Q_{sca}, and Q_{ext} for SiO_2, ZnO, and C are computed using the BHMIE subroutine [24] and are shown in Fig. 3 as functions of particle radius a. Note that Q_{abs} is zero for SiO_2 for any particle radius a as a consequence of the negligible imaginary part of m_{SiO_2}, and hence $\sigma_{sca,SiO_2} = \beta_{SiO_2}$. Q_{abs} is very small for ZnO due to significant semi-transparency of ZnO at 632.8 nm. Fig. 4 shows Φ for SiO_2, ZnO, and C, integrated over all radii, as a function of the scattering angle θ_{sca}. Table 3 lists the scattering and extinction coefficients of unmixed SiO_2, ZnO and C powders obtained by using Eq. (4) for $f_{v,i}^m \equiv f_{v,i}$. Also shown are the values obtained by applying the monodispersed approximation to Eq. (4) [22],

$$\{\kappa_i, \sigma_{\mathrm{sca},i}, \beta_i\} = \frac{0.75 f_{v,i}}{a}\left\{Q_{\mathrm{abs},i}(a), Q_{\mathrm{sca},i}(a), Q_{\mathrm{ext},i}(a)\right\}, \tag{7}$$

[1] The spectral subscript λ is omitted in the notation for brevity throughout the paper.

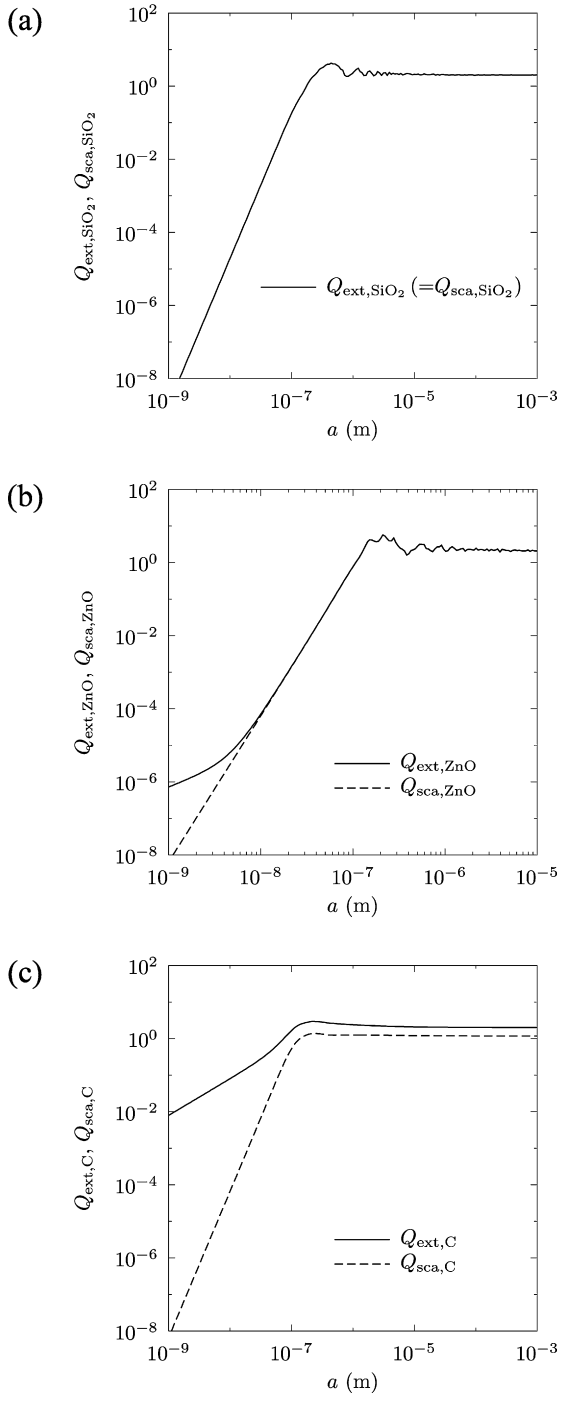

Fig. 3. Extinction and scattering efficiency factors of SiO_2, ZnO, and C particles as a function of particle radius, obtained by applying Mie theory.

where $a \equiv a_{50}$ or $a \equiv a_{32}$. Since the agreement between the results for poly- and monodispersed particles is reasonable only for SiO_2, the radiative properties employed in the numerical simulations are those obtained for polydispersions. Because of the uncertainty of the measured particle size distribution for ZnO, the effect of varying by 5% the parameters B, γ, and δ was examined on the extinction coefficient β_{ZnO}. Results of this sensitivity analysis are shown in Table 4. As expected after inspecting Eq. (1), the variation of δ has the strongest influence on β_{ZnO}. The variation by 5% of both the real and imaginary parts of m_{ZnO} and m_{C}, and the real part of m_{SiO} has a negligible effect on the radiative properties.

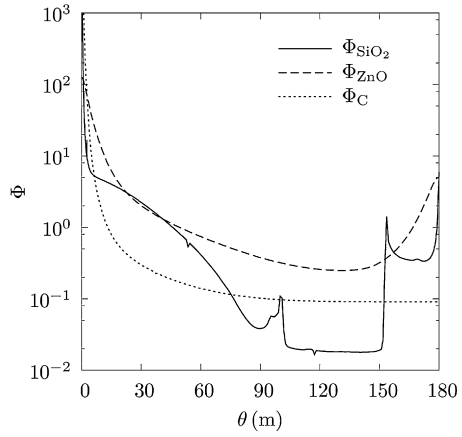

Fig. 4. Scattering phase functions $\Phi(\theta)$ of polydispersed SiO_2, ZnO, and C particles as a function of the scattering angle, obtained by applying the Mie solution.

Table 3
Scattering and extinction coefficients of unmixed SiO_2, ZnO and C powders obtained by applying Mie theory.

i	Dispersion	$\sigma_{\mathrm{sca},i}$ (m^{-1})	β_i (m^{-1})
SiO_2	mono, a_{50}	3823	3823
	mono, a_{32}	3719	3719
	poly	3705	3705
ZnO	mono, a_{50}	138983	139341
	mono, a_{32}	317611	317914
	poly	214364	214708
C	mono, a_{50}	4262	7327
	mono, a_{32}	4817	8283
	poly	9509	16591

Table 4
Sensitivity analysis by 5% variation of the particle size distribution parameters (Eq. (1)) on the extinction coefficient β_{ZnO} (in m^{-1}).

Parameter	·0.95	·1.00	·1.05
B	176052	214708	259465
γ	228850	214708	201239
δ	381684	214708	124718

4. Monte Carlo analysis

The collision-based ray-tracing Monte Carlo (MC) method is applied to solve for overall transmittance through packed-bed samples, defined as [7,20,21],

$$T \equiv \frac{\dot{Q}}{\dot{Q}_0}, \tag{8}$$

where $\dot{Q}$ and $\dot{Q}_0$ are the radiative power acquired by the fiber optics (#7 in Fig. 1) with and without a sample present in the sample holder, respectively. A large number of stochastic rays $N_{\mathrm{rays}} = 10^6$ is launched uniformly on a circular disc above the sample. A generic ray can undergo multiple scattering or absorption in the medium. The path length s to a scattering/absorption event is computed via [20,21],

$$s = -\frac{1}{\sum_{i=1}^{n} \beta_i^{\mathrm{m}}} \ln \Re_s. \tag{9}$$

If

$$\Re_\omega \geqslant \frac{\sum_{i=1}^{n} \sigma_{\mathrm{sca},i}^{\mathrm{m}}}{\sum_{i=1}^{n} \beta_i^{\mathrm{m}}}, \tag{10}$$

absorption occurs and the history of the ray is terminated. Otherwise, the scattering medium component k and the scattering direction $(\theta_{\text{sca}}, \phi_{\text{sca}})$ are determined according to,

$$\sum_{i=1}^{k-1} \sigma_{\text{sca},i}^{\text{m}} \leqslant \Re_k \sum_{i=1}^{n} \sigma_{\text{sca},i}^{\text{m}} < \sum_{i=1}^{k} \sigma_{\text{sca},i}^{\text{m}}, \tag{11}$$

$$\Re_{\varphi_{\text{sca}}} = \frac{\varphi_{\text{sca}}}{2\pi}; \qquad \Re_{\theta_{\text{sca}}} = \frac{1}{2} \int_0^{\theta_{\text{sca}}} \Phi_k(\theta) \sin\theta \, \mathrm{d}\theta. \tag{12}$$

When s exceeds the path length to the medium boundaries, reflection/absorption occurs at the walls assumed grey and diffuse with total hemispherical reflectivity $\rho = 0.5$. A ray reaching the upper free medium boundary is lost. Ray tracing in the supporting window and the focusing lens is performed by accounting for refraction and reflection at outer and inner surfaces using Snell's law and Fresnel's equations for non-absorbing media, respectively,

$$n_{\text{in}} \sin\theta_{\text{in}} = n_{\text{refr}} \sin\theta_{\text{refr}}, \tag{13}$$

$$\rho' = \frac{1}{2}\left[\left(\frac{\cos\theta_{\text{in}}/\cos\theta_{\text{refr}} - n_{\text{in}}/n_{\text{refr}}}{\cos\theta_{\text{in}}/\cos\theta_{\text{refr}} + n_{\text{in}}/n_{\text{refr}}}\right)^2 + \left(\frac{\cos\theta_{\text{refr}}/\cos\theta_{\text{in}} - n_{\text{in}}/n_{\text{refr}}}{\cos\theta_{\text{refr}}/\cos\theta_{\text{in}} + n_{\text{in}}/n_{\text{refr}}}\right)^2\right], \tag{14}$$

where θ_{in} and θ_{refr} are the cone angles of incidence and refraction, respectively, and n_{in} and n_{refr} are the refractive indices of the media the ray traverses before and after refraction, respectively. The refractive indices of both the supporting window and the lens glass are assumed to be equal 1.515. Finally, Eq. (8) is approximated by

$$T \approx \frac{N}{N_0}, \tag{15}$$

where N and N_0 are the numbers of rays intercepted by the fiber optics with and without a sample present in the sample holder, respectively.

5. Experimental and numerical results

All radiative properties of mixture components i reported in this section refer to volume fractions of unmixed powders, $f_{v,i}$, given in Table 1. The actual values employed in the simulations are based on $f_{v,i}^{\text{m}}$, corresponding to compositions of Table 2. The numerically calculated and experimentally measured overall transmittance T for samples 1–5 is shown in Figs. 5–7. Each experimental data point in Figs. 5–7 represents an average of 10 measurements [7].

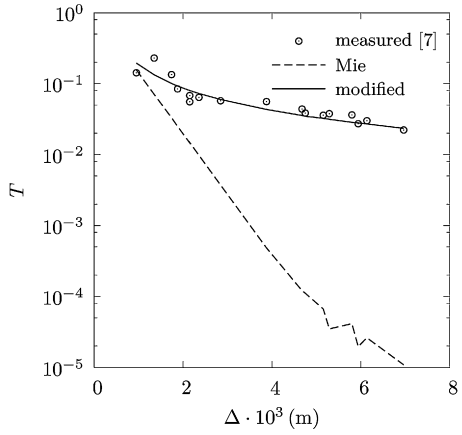

Fig. 5. Numerically calculated and experimentally measured overall transmittance of sample 1.

Fig. 5 shows T for sample 1. The numerical values of T obtained for Mie-based β_{SiO_2} and Φ_{SiO_2} follow approximately an exponential trend (Bouguer's law) and are significantly lower than those obtained experimentally. This implies that the contribution of incoming scattering, which in turn is a result of multiple scattering within the medium, is under-predicted by the MC simulation. Good agreement was obtained for β_{SiO_2}, increased by approximately one order of magnitude, and the Mie phase function amplified into the forward direction. However, the fraction of forward-scattered radiation was still insufficient to avoid the underestimation of T for thicker samples. Thus, an approximate phase function that matches the experimentally observed strong preference for forward scattering is constructed as

$$\Phi_{SiO_2}^*(\theta) = \begin{cases} \dfrac{\pi}{\theta_{\text{max},SiO_2}} \dfrac{\sin\left(\frac{\pi}{\theta_{\text{max},SiO_2}}\theta\right)}{\sin\theta}, & \theta \leqslant \theta_{\text{max},SiO_2}, \\ 0, & \theta > \theta_{\text{max},SiO_2} \end{cases} \tag{16}$$

which leads to $\beta_{SiO_2} = 3800\ \text{m}^{-1}$ and $\theta_{\text{max},SiO_2} = 0.70°$. These values are used for SiO_2 in simulations of samples 2–5. The relative difference between the Mie-based and $\Phi_{SiO_2}^*$-based β_{SiO_2} is 2.56%.

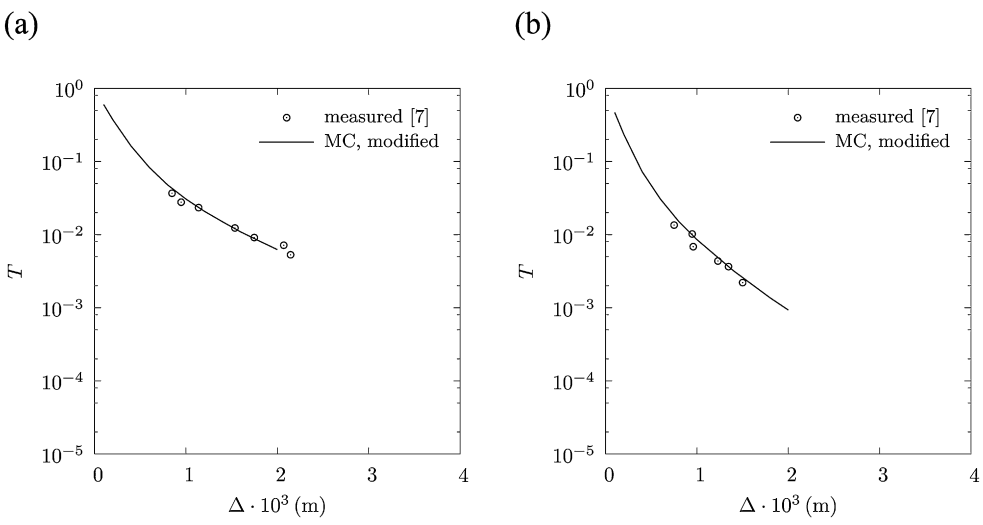

Fig. 6. Numerically calculated and experimentally measured overall transmittance of (a) sample 2 and (b) sample 3.

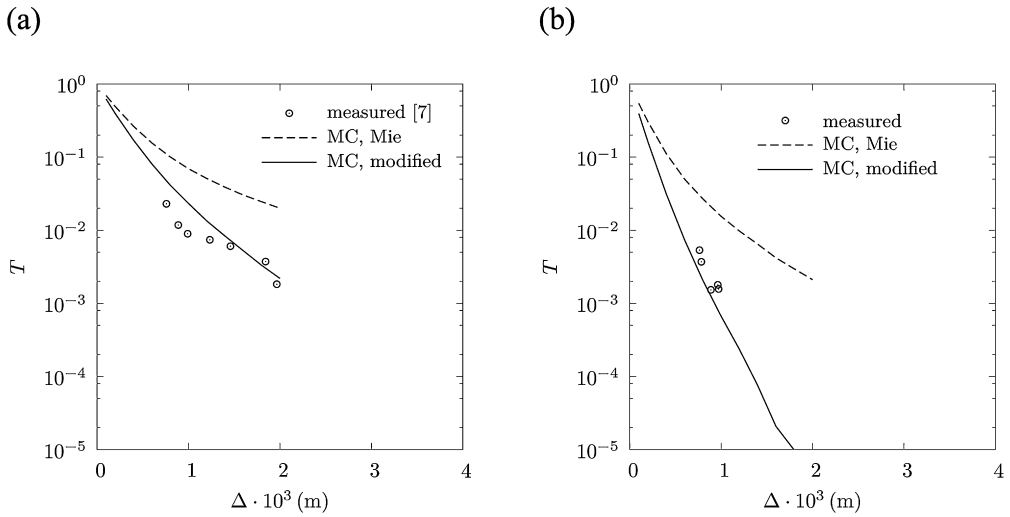

Fig. 7. Numerically calculated and experimentally measured overall transmittance of (a) sample 4 and (b) sample 5.

Figs. 6a and 6b show T for samples 2 and 3, respectively. Note that for both samples, T computed using Mie-based $\sigma_{\mathrm{sca,ZnO}}$, β_{ZnO} and Φ_{ZnO} is in the range 10^{-6}–10^{-5} and hence omitted from the plot. This drastic underestimation of T is explained by the very high values of $\sigma_{\mathrm{sca,ZnO}}$ and β_{ZnO} leading to significant off-scattering from the main optical axis z in the simulation. The phase function obtained by applying the Mie theory is only slightly modified by enhancing the forward-scattering fraction, leading to a modified phase function Φ^{**}_{ZnO},

$$\Phi^{**}_{\mathrm{ZnO}}(\theta) = \frac{2\Phi^{*}_{\mathrm{ZnO}}(\theta)}{\int_0^{\pi} \Phi^{*}_{\mathrm{ZnO}}(\theta)\sin\theta\,\mathrm{d}\theta};$$

$$\Phi^{*}_{\mathrm{ZnO}}(\theta) = \begin{cases} \zeta\,\Phi_{\mathrm{ZnO}}(\theta), & \theta \leqslant \theta_{\mathrm{max,ZnO}}, \\ \Phi_{\mathrm{ZnO}}(\theta), & \theta > \theta_{\mathrm{max,ZnO}}. \end{cases} \tag{17}$$

The simultaneous variation of $\sigma_{\mathrm{sca,ZnO}}$, β_{ZnO}, and Φ_{ZnO} in the simulations of samples 2 and 3 led to $\beta_{\mathrm{ZnO}} = 39000\ \mathrm{m}^{-1}$, $\sigma_{\mathrm{sca,ZnO}} = 37800\ \mathrm{m}^{-1}$, $\theta_{\mathrm{max,ZnO}} = 1°$, and $\zeta = 400$. As seen in Fig. 6, an excellent agreement with the experimental data is achieved for these values. The phase function of Eq. (17) is further used in the simulations of samples 4 and 5. The relative differences between the Mie-based and Φ^{**}_{ZnO}-based β_{ZnO} and ω_{ZnO} are −81.84 and −2.92%, respectively.

Fig. 7 shows T for samples 4 and 5. Note that in contrast to samples 1–3, T obtained for Mie-based β_{C}, $\sigma_{\mathrm{sca,C}}$ and Φ_{C} is overestimated. Since C is highly absorbing, the effect of incoming scattering becomes less important with increasing content of C [7], and hence, it is anticipated that Φ has a smaller influence on T. Moreover, the volume fractions of C in samples 4 and 5 are relatively small and variations of $\sigma_{\mathrm{sca,C}}$ and β_{C} do not influence the computed transmittance significantly. However, it was observed during the preparation of the samples that C darkens the surface of ZnO particles during the mixing process. Hence, the extinction coefficient of ZnO was decreased from the Mie-based value to $\beta_{\mathrm{ZnO}} = 67800\ \mathrm{m}^{-1}$ (by 68%) for samples 4 and 5 to account for the increased absorption, while the scattering coefficient was kept unchanged at $\sigma_{\mathrm{sca,ZnO}} = 37800\ \mathrm{m}^{-1}$. This led to reasonably good agreement with the experimental results.

The required decrease of β_{ZnO} and ω_{ZnO} as compared to the Mie-based values for samples 2–5 is attributed to the dependent scattering effects affecting the small ZnO particles packed in the void space between the large SiO_2 particles [23,29,30]. The heterogeneous character of all samples, the non-spherical shape of the densely packed SiO_2 and C particles, and the dependent scattering effects affecting them [16–18], further lead to the observed discrepancies.

The MC computation accuracy is assessed by calculating the relative mean standard deviation of the overall transmittance $S_{\bar{T}}/\overline{T}$ for sample #5 [20,21]. Separate MC simulations, performed for 10 ray sub-samples each containing 10^5 rays generated for a different set of random numbers, lead to $S_{\bar{T}}/\overline{T} = 0.065$.

6. Summary and conclusions

Radiative characteristics of packed-bed mixtures containing polydispersed SiO_2, ZnO and C particles were determined numerically by employing the Monte Carlo technique and validated experimentally by comparing the computed and measured overall transmittance. In the first approach, the Mie theory was applied to compute the scattering and extinction coefficients and the scattering phase functions of independently-scattering particles, which led to an underestimated transmittance for highly-scattering samples containing SiO_2 and ZnO, and to overestimated transmittance for highly-absorbing samples containing—in addition—C. Reasonable agreement between the experimentally measured and numerically computed values of the transmittance was achieved when incorporating approximate phase functions for SiO_2 and ZnO particles that matched the experimentally observed preference for forward scattering and an augmented absorption coefficient of ZnO that accounted for darkening by added carbon particles.

Future studies will focus on directional-spectral measurements at high temperatures to determine the radiative properties of porous materials encountered in solar thermochemical reactors, such as packed beds of ZnO, C and $CaCO_3$, and reticulate porous ceramics.

Acknowledgements

This work has been financially supported by the Swiss National Science Foundation under contracts No. 200021-115888 and No. PP002-114713. We thank T. Brzović for the preliminary calculations.

References

[1] A. Steinfeld, R. Palumbo, Solar Thermochemical Process Technology, in: R.A. Meyers (Ed.), Encyclopedia of Physical Science and Technology, vol. 15, Academic Press, San Diego, 2001, pp. 237–256.

[2] W. Lipiński, A. Steinfeld, Heterogeneous decomposition under direct irradiation, International Journal of Heat and Mass Transfer 47 (2004) 1907–1916.

[3] T. Osinga, G. Olalde, A. Steinfeld, The solar carbothermal reduction of ZnO—Shrinking packed-bed reactor modeling and experimental validation, Industrial & Engineering Chemistry Research 43 (2004) 7981–7988.
[4] R. Müller, W. Lipiński, A. Steinfeld, Transient heat transfer in a directly-irradiated solar chemical reactor for the thermal dissociation of ZnO, Applied Thermal Engineering 28 (2008) 524–531.
[5] N. Piatkowski, A. Steinfeld, Solar-driven coal gasification in a thermally irradiated packed-bed reactor, Energy and Fuels 22 (2008) 2043–2052.
[6] T. Osinga, W. Lipiński, E. Guillot, G. Olalde, A. Steinfeld, Experimental determination of the extinction coefficient for a packed-bed particulate medium, Experimental Heat Transfer 19 (2006) 69–79.
[7] W. Lipiński, E. Guillot, G. Olalde, A. Steinfeld, Transmittance enhancement of packed-bed particulate media, Experimental Heat Transfer 21 (2008) 73–82.
[8] B.M. Agarwal, M.P. Mengüç, Forward and inverse analysis of single and multiple scattering of collimated radiation in an axisymmetric system, International Journal of Heat and Mass Transfer 34 (1991) 633–647.
[9] D. Baillis, J.-F. Sacadura, Thermal radiation properties of dispersed media: theoretical prediction and experimental characterization, Journal of Quantitative Spectroscopy and Radiative Transfer 67 (2000) 327–363.
[10] K. Kamiuto, M. Iwamoto, T. Nishimura, M. Sato, Radiation-extinction coefficients of packed-sphere systems, Journal of Quantitative Spectroscopy and Radiative Transfer 45 (1991) 93–96.
[11] P.D. Jones, D.G. McLeod, D.E. Dorai-Raj, Correlation of measured and computed radiation intensity exiting a packed bed, Journal of Heat Transfer 118 (1996) 94–102.
[12] R. Lopes, L.M. Moura, D. Baillis, J.-F. Sacadura, Directional spectral emittance of a packed bed: correlation between theoretical prediction and experimental data, Journal of Heat Transfer 123 (2001) 240–248.
[13] J. Kuhn, S. Korder, M.C. Arduini-Schuster, R. Caps, J. Fricke, Infrared-optical transmission and reflection measurements on loose powders, Review of Scientific Instruments 64 (1993) 2523–2530.
[14] A. Ishimaru, Y. Kuga, Attenuation constant of a coherent field in a dense distribution of particles, Journal of the Optical Society of America 72 (1982) 1317–1320.
[15] L. Hespel, S. Maiguy, J.-J. Greffet, Radiative properties of scattering and absorbing dense media: theory and experimental study, Journal of Quantitative Spectroscopy and Radiative Transfer 77 (2003) 193–210.
[16] B.P. Singh, M. Kaviany, Independent theory versus direct simulation of radiation heat transfer in packed beds, International Journal of Heat and Mass Transfer 34 (1991) 2869–2882.
[17] R. Coquard, D. Baillis, Radiative characteristics of opaque spherical particles beds: a new method of prediction, Journal of Thermophysics and Heat Transfer 18 (2004) 178–186.
[18] R. Coquard, D. Baillis, Radiative characteristics of beds of spheres containing an absorbing and scattering medium, Journal of Thermophysics and Heat Transfer 19 (2005) 226–233.
[19] T. Williams, C. Kelley, GNUPLOT: An Interactive Plotting Program, version 4.0, 2004, http://www.gnuplot.info/documentation.html.
[20] M.F. Modest, Radiative Heat Transfer, second edition, Academic Press, San Diego, 2003.
[21] J.T. Farmer, J.R. Howell, Comparison of Monte Carlo strategies for radiative transfer in participating media, in: J.P. Harnett, T.F. Irvine (Eds.), Advances in Heat Transfer, vol. 31, Academic Press, San Diego, 1998, pp. 333–429.
[22] L.A. Dombrovsky, Radiation Heat Transfer in Disperse Systems, Begell House, New York, 1996.
[23] C.L. Tien, B.L. Drolen, Thermal radiation in particulate media with dependent and independent scattering, Annual Review of Numerical Fluid Mechanics and Heat Transfer 1 (1987) 1–32.
[24] C.F. Bohren, D.R. Huffman, Absorption and Scattering of Light by Small Particles, John Wiley & Sons, Inc., New York, 1983.
[25] E. Palik, Handbook of Optical Constants of Solids, vol. 1, Academic Press, San Diego, 1985.
[26] J. Springer, A. Poruba, M. Vanecek, S. Fay, L. Feitknecht, N. Wyrsch, J. Meier, A. Shah, T. Repmann, O. Kluth, H. Stiebig, B. Rech, Improved optical model for thin film silicon solar cells, in: Proceedings of the 17th European Photovoltaic Solar Energy Conference, Munich, 2001, pp. 2830–2835.
[27] B.Y.H. Liu, W.W. Szymanski, D.Y.H. Pui, Response of laser optical particle counter to transparent and light absorbing particles, ASHRAE Transactions 92 (1986) 518–538.
[28] A. Quarteroni, R. Sacco, F. Saleri, Numerical Mathematics, Springer-Verlag, New York, 2000.
[29] S.G. Tinsley, A. Bowman, Rutile type titanium pigments, Journal of the Oil and Color Chemist's Association 32 (1949) 233–270.
[30] T. Kunitomo, Y. Tsuboi, H.M. Shafey, Dependent scattering and dependent absorption of light in a fine-particle dispersed medium, Bulletin of the JSME 28 (1985) 854–859.